



**HAL**  
open science

## Laboratory study on hygrothermal behavior of three external thermal insulation systems

M. Bendouma, T. Colinart, P. Glouannec, H. Noël

### ► To cite this version:

M. Bendouma, T. Colinart, P. Glouannec, H. Noël. Laboratory study on hygrothermal behavior of three external thermal insulation systems. *Energy and Buildings*, 2020, 210, pp.109742 -. 10.1016/j.enbuild.2019.109742 . hal-03489810

**HAL Id: hal-03489810**

**<https://hal.science/hal-03489810>**

Submitted on 21 Jul 2022

**HAL** is a multi-disciplinary open access archive for the deposit and dissemination of scientific research documents, whether they are published or not. The documents may come from teaching and research institutions in France or abroad, or from public or private research centers.

L'archive ouverte pluridisciplinaire **HAL**, est destinée au dépôt et à la diffusion de documents scientifiques de niveau recherche, publiés ou non, émanant des établissements d'enseignement et de recherche français ou étrangers, des laboratoires publics ou privés.



Distributed under a Creative Commons Attribution - NonCommercial 4.0 International License

# Laboratory study on hygrothermal behavior of three external thermal insulation systems

M. BENDOUMA<sup>1</sup>, T. COLINART<sup>1\*</sup>, P. GLOUANNEC<sup>1</sup>

<sup>1</sup> Univ. Bretagne Sud, UMR CNRS 6027, IRDL, F-56100 Lorient, France

## Corresponding author:

Thibaut COLINART

IRDL – Université de Bretagne Sud

Rue de saint Maudé, BP 92116,

56321 Lorient Cedex, France

Phone: 33/0 2 97 87 45 17

Fax: 33/0 2 97 87 45 72

Mail : thibaut.colinart@univ-ubs.fr

## **Abstract**

This work focuses on the hygrothermal behavior of three external thermal insulation systems: one ETICS including EPS insulation and two ventilated cladding systems including either mineral or biobased insulation. These systems were applied on a rendered hollow concrete wall and tested simultaneously between two climatic chambers. Thermocouples, humidity sensors and heat flux sensors allow investigating the hygrothermal behavior of the retrofitted wall at different stages: just after the application of insulations systems, during safe and critical use. The measured data are compared to numerical results obtained by solving a heat and moisture transfer model.

Results highlight the key role of adhesive on ETICS, which provides a significant moisture source during the application and forms an additional moisture transfer resistance within the wall. Results on ventilated cladding systems show that using biobased insulation may delay and even prevent the risk of interstitial condensation. The comparison between numerical and experimental results is satisfying for temperature and heat flow density, but underline the sensitivity of relative humidity to the sorption capacity of hygroscopic building materials. In addition, the systems design has a great influence on the condensation risks.

## **Keywords**

ETICS; Ventilated cladding; Heat and moisture transfer; Interstitial condensation; Hygrothermal simulation; Bio-based Insulation;

**Highlights:**

- Adhesive used for ETICS provides moisture within the wall and increases moisture transfer resistance.
- Simulated temperature and relative humidity profiles agree with the measured ones.
- Using bio-based insulation may reduce the condensation risk.
- The ventilated cladding system design is of high importance regarding the condensation risk.

# 1 Introduction

In France, dwellings built between 1950 and 2000 represent around 50 % of residential building stock. They are made mainly with masonry and are characterized by low or inexistent thermal insulation [1]. In the view of achieving high energy performance, safe and efficient refurbishment of external walls have to be undertaken. For now, External Thermal Insulation Composite Systems (ETICS) and ventilated cladding systems are widespread techniques. Depending on the building types and the climatic conditions, they are designed to fulfil minimal thermal and acoustic performance and fire resistance. Examples of building renovation with external thermal insulation can be found in [2-4].

Nevertheless, one of the major concerns with external thermal insulation is moisture performance and its consequences [5]. For instance, ETICS wetting occurs obviously by driving rain [6], but also by surface condensation when wall external surface temperature drops below the dew point of the air in consequence of long-wave radiation exchanges [7]. If the drying is not sufficiently fast, high moisture content on surfaces may reduce service-life and durability of ETICS. In this view, numerous numerical studies aimed to evaluate short-term risk of surface condensation [8-12] and long-term risk of carbonation and corrosion of reinforcement of ETICS [13-14]. Recently, it was expected that installing a cladding instead of a rendering may reduce the risks [15]. However, the validation of this conclusion is rather difficult: when available, the experimental data are monitored on real buildings over years and their comparison with numerical results underline the great influence of building orientation, radiative properties, but also hygric properties of thermal insulation layer and exterior plaster. To limit the influence of unknown or hazardous phenomenon, like weather, there is therefore a need to collect experimental data in well-controlled conditions i.e. in climatic chambers or specially built test facilities like hot-box [16]. To date, temperature profiles, thermal

resistance (or U-value) and thermal behavior were evaluated mainly for ETICS [17-23] under static and dynamic climate [17, 21-23], under accelerated ageing [18] or even under high temperature-rain simulation test [19, 20]. In most of these studies, moisture is expected to influence the thermal behavior. Unfortunately, none of them focused on the hygrothermal behavior of the walls in the hygroscopic range. On the other hand, hygric behavior in the capillary range was studied by Hens and Carmeliet [24] and Barreira et al. [25] by monitoring mass changes during the drying stage: Hens and Carmeliet [24] noted that a wet massive brick wall may take a considerable time before drying all its built-in moisture, while Barreira et al. [25] observed a rather fast drying kinetic of ETICS itself. Regarding ventilated cladding systems, their hygrothermal behavior was investigated experimentally in a context of lightweight building as reviewed by Busser et al. [26]. However, no laboratory experiments in a context of external thermal insulation was found in the literature.

Therefore, the current paper proposes a laboratory investigation of thermal and hygrothermal behavior of two ventilated cladding systems applied on a rendered hollow concrete block wall. For comparison purpose, ETICS is also studied. Particularly, the performances of these three external thermal insulation systems are evaluated during different stage of their service-life: during the application of thermal insulation, the consequences in terms of humidity are evaluated; in normal use, thermal resistances are estimated and compared to theoretical ones, while the hygrothermal behavior is measured in the view of validating heat and moisture transfer model; last, risk of condensation is investigated for ventilated cladding systems and the design of the systems is questioned. In this view, the paper is divided as follows: Section 2 presents the three external thermal insulation systems studied, their instrumentation and the hygrothermal model; in Section 3, experimental evidences are pointed out during the application of the insulation systems and under steady state; Section 4 deals with the transient hygrothermal behavior and the numerical results for ventilated cladding systems.

## 2 Materials and methods

### 2.1 External Thermal Insulation systems

Three External Thermal Insulation (ETI) systems are applied on a wall with dimensions of 2 x 2.1 x 0.21 m made of hollow concrete block and cement mortar and rendered on its outer face with a lime-based render (*VPI Monolor ZF*).

The first system is an ETICS made of double EPS panels, a 10 mm thick coarse hydraulic plaster layer (*Parexlanko EHI GM*) and a 5mm thick siloxane finishing plaster layer on its outer face (*Parexlanko Revlane+ siloxané Ignifugé TF*). ETICS is bonded to the wall substrate with a 3 mm thick hydraulic mortar (*Parexlanko Maite*) and supplementary mechanical anchors, which corresponds to a wet construction method. Note here that EPS panels are glued together with acrylic glue (*PRB Col Wood*) despite it does not correspond to common practice.

The two other systems are ventilated cladding systems. Their design consists, from the interior to the exterior, of an OSB board, a first insulation layer, which is integrated into a wooden frame, an airtight rainscreen membrane, a ventilated cavity and a cladding. This design comes from timber frame buildings where OSB board acts as a bracing system and vapor barrier. These systems are fixed with metal brackets only, which corresponds to a dry construction method. To ensure continuity of thermal insulation between the existing wall and OSB board, an adaption insulation layer is added. Different insulating and cladding materials are tested in these two systems. In the first one, biobased and hygroscopic materials are used: wood cladding, wood wool as first insulation layer and loose-fill cellulose as adaption insulation layer. Ventilating cladding systems using these materials has been tested on site by Capener et al. [27]. In the second one, less hygroscopic building materials are used: fibre-cement cladding and glass wool as insulation layers. This system has been tested on site in

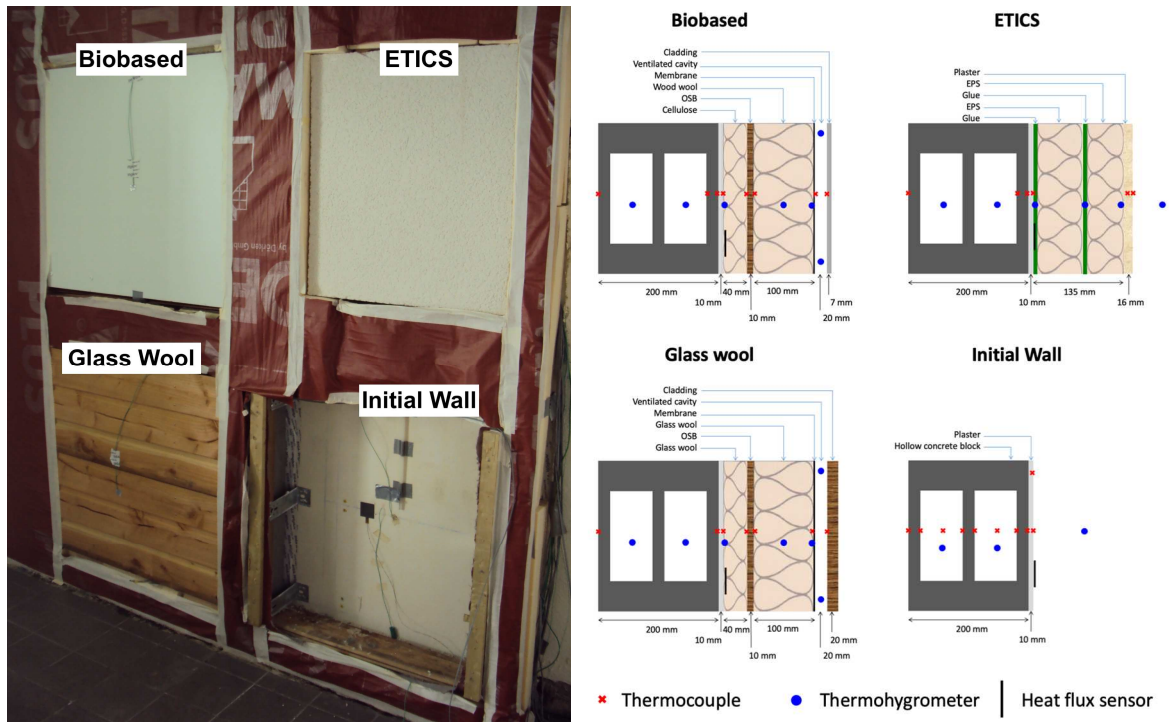
previous paper [28]. Similar systems are also tested by Capener et al. [27] or Pihelo et al. [29]. Last, note that ventilated cavity of both systems is 20 mm width: even if it is narrower than 40 mm, the most observed width in the literature, narrow cavities are not unusual for such systems [27,29-33].

Table 1 gathers systems dimensions, theoretical thermal resistances  $R_{th}$  and hydric resistance  $R_{hyd}$  (defined as the sum of each  $S_d$ ) calculated with in-lab measured hygrothermal properties (see Annex 1 for protocols and results). All systems present similar thicknesses and thermal resistances  $R_{th}$  higher than  $3.5 \text{ K.m}^2.\text{W}^{-1}$ . Hydric resistance of ETICS is much higher due to the high water vapor diffusion resistance factor of EPS. Last, their surfaces were set to avoid edge and side effects. Since the systems do not cover the entire wall surface, all gaps between the systems are filled with polyurethane insulation, except one part of rendered hollow concrete block wall which is kept non-insulated for comparison purpose. It was verified that the thermal behavior of the retrofitted wall is fairly homogeneous and mutual interactions between the systems is limited. A view of the tested wall is presented in Figure 1a.

	Thickness [m]	Surface [m <sup>2</sup> ]	$R_{th}$ [K.m <sup>2</sup> .W <sup>-1</sup> ]	$R_{hyd}$ [m]
<i>ETICS</i>	0.151	0.6 x 0.6	3.9	5.9
<i>Glass Wool</i>	0.15	0.8 x 0.8	4.1	1
<i>Biobased</i>	0.15	0.8 x 0.8	3.5	1.2

**Table 1: Dimensions, theoretical thermal and hydric resistance of the external thermal insulation systems.**

For sake of simplicity, each ETI systems is noted *ETICS*, *Glass Wool* and *Biobased* respectively and the non-insulated part is noted *Initial Wall* in the rest of the paper. The entire rendered hollow concrete block wall is noted *RHCB wall*.



*Figure 1:View (a), design and instrumentation (b) of the tested walls.*

## 2.2 Experimental set-up

The wall with external insulation systems is tested between two climatic chambers. The junctions between the wall and the chambers are sealed with polyurethane foam. In each chamber, temperature and relative humidity are controlled by heater, refrigeration equipment and steam vaporizer. More details about the set-up can be found in [34].

Capacitive humidity sensors (Sensirion SHT 75, Staefa, Switzerland) are used to monitor temperature and relative humidity with a precision of 0.5 °C and 2 % respectively. Several sensors are inserted at different depths within the walls (see Figure 1b). Attention is paid to place them in the central part of each system and in front of a cavity of hollow concrete block. These sensors provide the conditions of small air pocket in equilibrium with surrounding materials. At the interior side, one sensor is placed in the center of the chamber and K thermocouple measures temperature at the opposite surface of climatic chambers. At the exterior side, conditions are measured in the center of the chamber and locally: sensors are

placed at 15 cm in front of *Initial wall* and *ETICS*; sensors are located at the inlet and outlet of the ventilated cavity for *Glass Wool* and *Biobased*. An omnidirectional anemometer (model 8465, TSI Incorporated, St. Paul, MN, USA) is used to measure air velocity at the same positions with a precision of  $\pm 2 \%$ . In addition, temperatures are measured at cladding' surfaces and at other surfaces of climatic chamber with K thermocouples. Last, heat flux sensors (Captec, Lille, France) are placed at the outer surface of *Initial Wall* and at the interfaces between ETI systems and *RHCB wall*. The relative uncertainty is evaluated at 15 % for heat flux density. All sensors are connected to dataloggers, which records the data every 10 minutes.

### 2.3 Hygrothermal modeling

Steady-state and transient hygrothermal simulations are performed to support the experimental observations. The constitutive equation for heat and moisture transfer in porous materials and for energy and mass balances in hollow concrete block cavities are reported in Annex 2. These equations are solved with Comsol Multiphysics for three geometries: *initial wall*, ETI systems alone and entire walls (see Figure 2).

At the boundaries, either Dirichlet condition or convection, long-wave radiation and latent exchanges are considered. The latter write:

$$\varphi_{T_{surf}} = h_{cv} (T_{surf} - T_{amb}) + \varepsilon \sigma (T_{surf}^4 - T_{surf,rad}^4) + \varphi_{m_{surf}} L_v \quad (1)$$

$$\varphi_{m_{surf}} = k_m \left( \frac{M_v}{R} \right) \left( \frac{\phi_{surf} p_{v,sat}(T_{surf})}{T_{surf}} - \frac{\phi_{amb} p_{v,sat}(T_{amb})}{T_{amb}} \right) \quad (2)$$

where mass convective exchange coefficient  $k_m$  is always deduced from convective thermal exchange coefficients  $h_{cv}$  by the Lewis relation [35] and where the material emissivity  $\varepsilon$  is measured in the lab (see Annex 1). The setting of other parameter is detailed hereafter as function of simulated geometry.

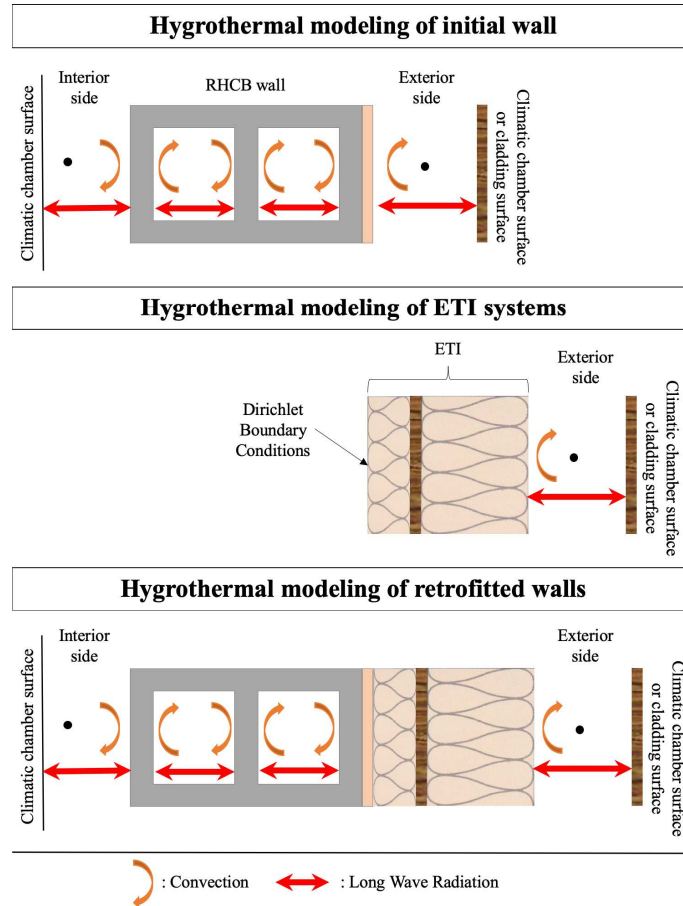


**Figure 2 : Overview of modeling approaches.**

### Hygrothermal modeling of *initial wall*

Because of the geometry of hollow concrete block, 2D-modeling approach is adopted. At the boundaries, ambient conditions  $T_{amb}$  and  $\phi_{amb}$  are the ones measured in the center of interior chamber and locally on the exterior side; convective thermal exchange coefficients  $h_{cv}$  were previously evaluated to  $5 \text{ W m}^{-2} \text{ K}^{-1}$  [34,36,37]; last, surface temperatures for long-wave radiation exchanges  $T_{surf,rad}$  are the ones measured at the opposite surface of climatic chambers.

Because of 2D modeling, inhomogeneous temperature and relative humidity fields are expected. Nevertheless, due to high vapor resistance and low thermal resistance of concrete, iso-values are almost parallel to height of the wall. Therefore, simulation results obtained at mid-cavity height are considered in the analysis.

### **Hygrothermal modeling of ETI systems**

Since ETI systems are made of homogeneous layers, 1D-modeling approach is adopted. Dirichlet boundary conditions are applied using temperature and relative humidity measured at the interfaces between *RHCB wall* and ETI systems. For *ETICS*,  $T_{amb}$  and  $\phi_{amb}$  are the ones measured locally;  $h_{cv}$  was previously evaluated to  $5 \text{ W m}^{-2} \text{ K}^{-1}$  [34,36,37];  $T_{surf,rad}$  is the one measured at the opposite surface of exterior climatic chamber. For ventilated cladding systems (*Glass Wool* and *Biobased* walls), outer boundary conditions are rather considered within the cavity: ambient conditions are the mean values between cavity inlet and outlet;  $h_{cv}$  is expected to depend on the local velocity;  $T_{surf,rad}$  is set to the cladding surface temperature.

### **Hygrothermal modeling of retrofitted walls**

Because of the geometry of hollow concrete block, 2D-modeling approach is adopted. Boundary conditions defined above are used on interior and exterior side. Furthermore, a perfect contact is assumed at the interfaces between *RHCB wall* and ETI systems, leading to the continuity of temperature and vapor pressure fields.

## **3 Experimental evidences**

### **3.1 Consequences of the application of ETI systems**

The *RHCB wall* is built 4 months before the application of ETI systems and conditioned under different temperature and humidity conditions until hygrothermal equilibrium is reached [38]. ETI systems are applied at  $t = 0$  (see Figure 3): *Glass Wool* and *Biobased* are completely build while only EPS panels are installed for *ETICS*, the plaster layers being applied 65 days later. Then, the walls are subjected to constant temperature and relative

humidity for 160 days: regulation set points are fixed to 10 °C / 55 % in the exterior side and 20 °C / 40 % in the interior side. Their variations are plotted in Figure 3. We observe that temperature set points are well respected, while relative humidity presents punctually fluctuations up to 15 %. Electrical failures of acquisition system lead to lack of less than 10 % of data around the 70<sup>th</sup> and the 115<sup>th</sup> days. However, set-points were kept in each climatic chamber during this time. Last, let note that the slight relative humidity increases observed around the 65<sup>th</sup> and the 95<sup>th</sup> days are only due to a temperature increase caused by an interruption in the regulation of the exterior side.

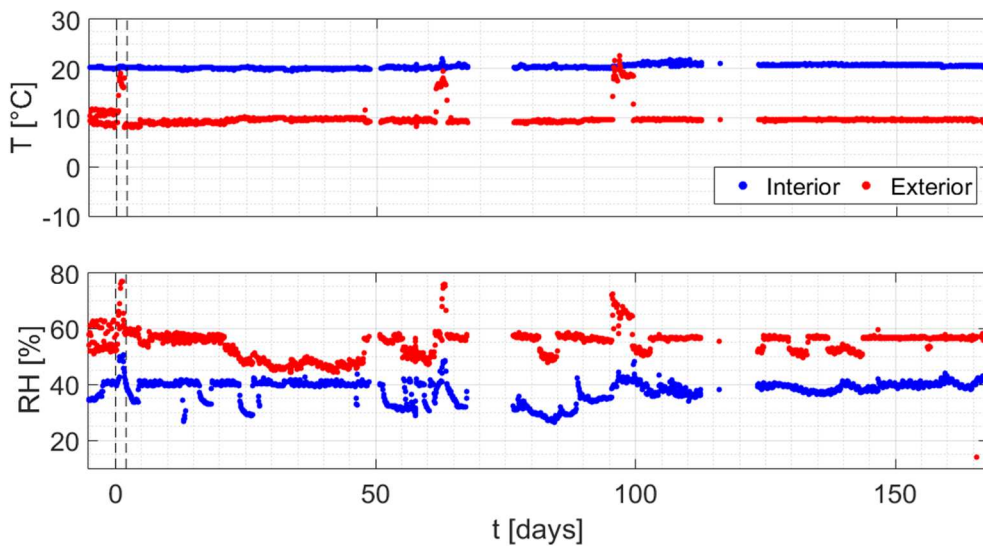


**Figure 3: Measured temperature and relative humidity at interior and exterior around the application of ETI systems.**

Figure 4 shows relative humidity variations measured in exterior cavities of the *RHCB wall* and at interfaces between *RHCB wall* and ETI systems. In addition, measured heat flux are presented. During the application of *ETICS*, moisture is provided by the adhesive, saturating thus air around the sensor at the interface. Then, this moisture source should be then evacuated outside the wall. Since hydric resistance of *ETICS* is much larger than the one of *RHCB wall*, moisture is preferentially transfer towards the interior side, as highlighted by the RH increase in the cavity during the first days. However, the drying is slow: relative humidity

decreases within the cavity after 25 days, while saturation is no more observed at the interface only after 35 days. Even after 160 days, a gradient exists within the wall, meaning that moisture transfer still occurs: hygric equilibrium is expected not to be reached for *ETICS*. On the other hand, the application of the ventilated cladding systems provides no additional moisture source, as highlight by the identical relative humidity levels in the cavity before and after  $t = 0$ . Because of the new boundary conditions applied after  $t = 0$ , relative humidities tend toward a new equilibrium state that is reached after 160 days. Last, the application of ETI systems leads to a significant reduction of heat losses: under the current conditions, heat flux decreases from approximately  $15 \text{ W}\cdot\text{m}^{-2}$  before insulation to less than  $3 \text{ W}\cdot\text{m}^{-2}$  after insulation. Because of low thermal inertia of ETI systems, thermal equilibrium is rapidly reached compared to hygric equilibrium.

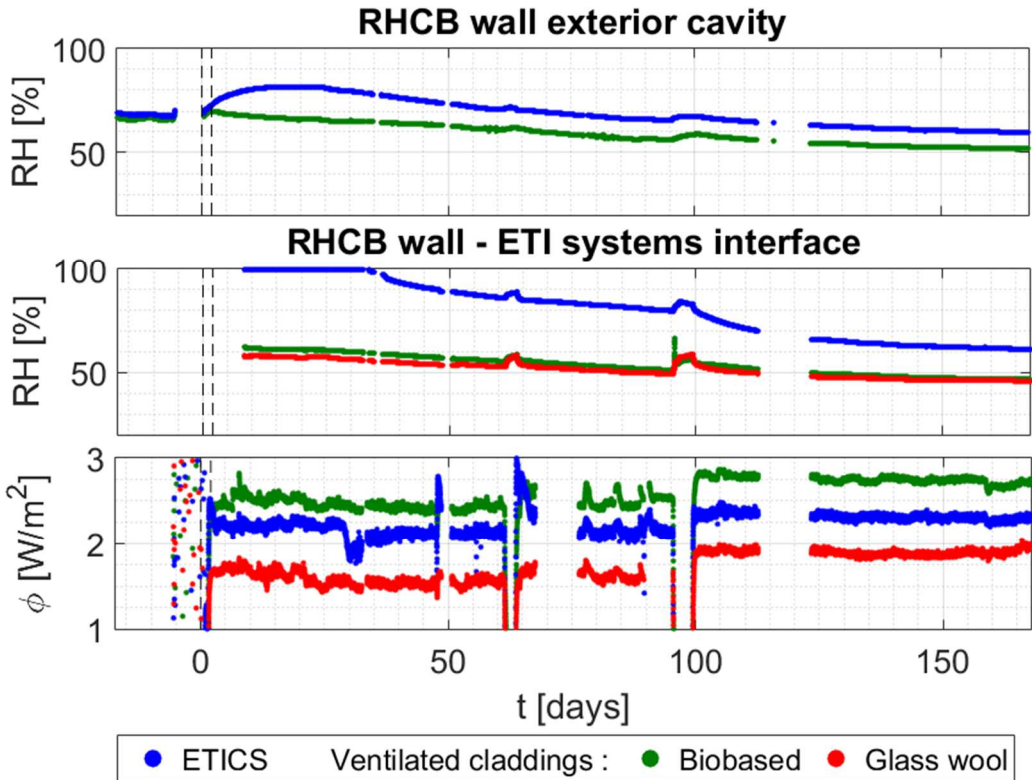


*Figure 4: Measured relative-humidity and heat flux density within the tested walls before and after the installation of ETI systems.*

### 3.2 Steady-state analysis

At the end of the previous test, a steady-state analysis is performed. Figure 5 show the temperature and relative humidity profiles for each ETI system and *Initial Wall*. The measurements are averaged over 6 hours and vertical errorbars represent the min and max values of the sequence. The simulated profiles are obtained by running hygrothermal models under steady state. Table 2 gathers thermal resistances evaluated from heat flux and temperature difference measurement according to the standard ISO 9869 [39]: temperature measured at interfaces between *RHCB wall* and ETI systems is used, excepted for *Initial Wall* for which interior surface temperature is used. These experimental resistances are compared to theoretical thermal resistance calculated according to the standard ISO 6946 [40].

A rather good agreement is observed for the temperature profiles and the thermal resistances of each ETI systems. The small differences observed for *Initial Wall* may be explained as follow. On the one hand, since thermal resistance is rather small, simulated profiles are very sensitive to thermal properties (thermal conductivity, emissivity or convective heat transfer coefficient) [41]. On the other hand, since temperature and heat flux sensors are directly in contact with air, large fluctuations due to the local boundary conditions are observed, which influences to some extent the evaluation of thermal resistance.

Regarding relative humidity, simulated profiles match with experiments for *Initial Wall* and ventilated cladding systems. However, large differences arise for *ETICS*, especially between EPS panels and at the interface between *RHCB wall* and *ETICS*. To apprehend the origin of these differences, a second profile is simulated by considering an additional hydric resistance due to the adhesive. Thickness and vapor diffusion resistance factor are set respectively to 1 mm and 3000 [42]. The simulated profile is slightly modified, but it is not sufficient to explain the differences between simulation and experiment. As previously mentioned, *ETICS*

dried out not entirely and steady-state is not reached, explaining the higher measured relative humidity levels compared to simulated ones.

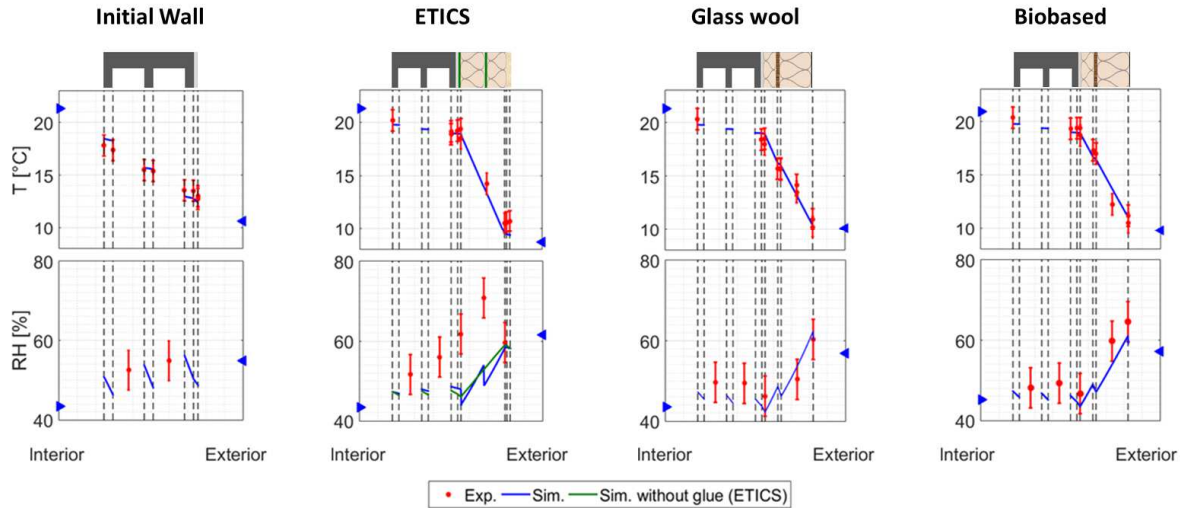


**Figure 5: Measured and simulated temperature and relative humidity profiles of the tested walls (►/◄measured air boundary conditions)**

$R_{th}$ [K.m <sup>2</sup> .W <sup>-1</sup> ]	Measured (ISO 9869)	Calculated
<i>Initial Wall</i>	0.29	0.35-0.41
<i>ETICS</i>	3.7	3.8
<i>Glass Wool</i>	4	4
<i>Biobased</i>	3	3.1

**Table 2: Measured and calculated thermal resistance of the Initial wall and ETI systems.**

## 4 Hygrothermal behaviour of ventilated cladding systems

This section aims to compare the measured and simulated hygrothermal behavior of the systems. Since ETICS has not reached hygrothermal equilibrium, its transient simulation is rather difficult, particularly due to the uncertainties in the initial conditions. Therefore, this section focuses only on *Glass Wool* and *Biobased* walls. Two experiments are performed: the

first one lead to hygrothermal safe conditions within the walls, while the second ones should lead to interstitial condensation.

## 4.1 Hygrothermal safe test

### 4.1.1 Experimental boundary conditions

This experiment is run directly just after the previous sequence (Figure 3) for more than 85 days. The measured boundary conditions are presented in Figure 6: at interior side, air temperature is correctly maintained at  $20 \pm 1$  °C, while air relative humidity fluctuates by 10 % around the 50 % set-point. At exterior side, air temperature and relative humidity change respectively from 9 to 26 °C and from 60 to 70 %. Due to regulation problems, exterior air relative humidity drops during few days around the 15<sup>th</sup> and the 45<sup>th</sup> day. Nevertheless, these fluctuations are still interesting in the view of testing models.

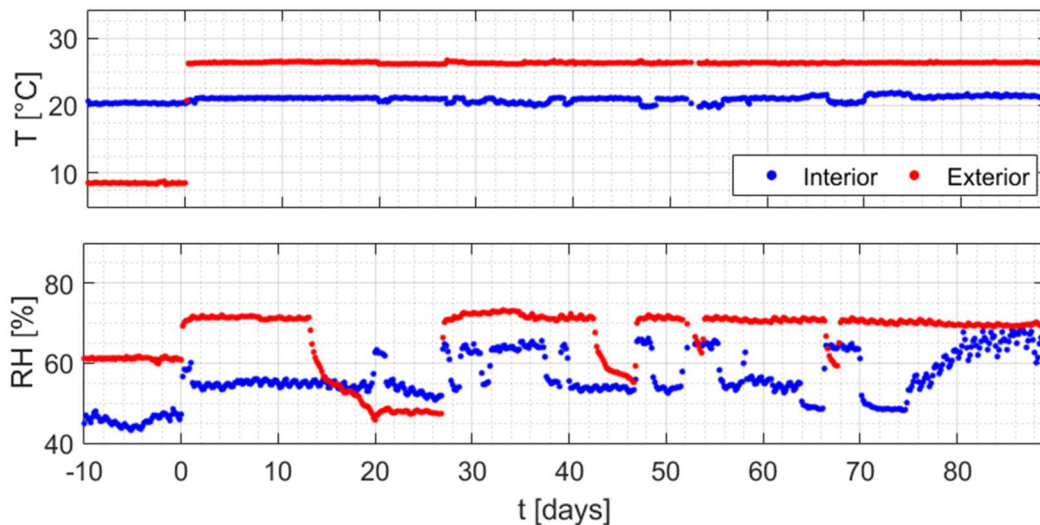


**Figure 6: Measured temperature and relative humidity at interior and exterior sides during hygrothermal safe test.**

In addition, air velocity is measured within the ventilated cavity of *Glass Wool*: it did not exceed  $0.2 \text{ m.s}^{-1}$  before the set-point change and  $0.04 \text{ m.s}^{-1}$  after. In ventilated cavity, air flows under the action of two driving forces: wind pressure and thermal buoyancy. In the

present experimental set-up, there is no wind and thermal gradient along the cavity height are small. Therefore, natural convection prevails in the ventilated cavity: convective thermal exchange coefficients  $h_{cv}$  is evaluated to  $5 \text{ W m}^{-2} \text{ K}^{-1}$  [43].

#### 4.1.2 Comparison between numerical and experimental results

This comparison occurs in two stages: hygrothermal model of ETI systems is run first, before the one of the entire wall (*RHCB wall* and ETI systems). Whatever the simulation, initial conditions are fixed by running a steady-state simulation before the set-point change since hygrothermal equilibrium is reached for these walls.

This methodology is applied hereafter for *Biobased* wall. Simulation is started 10 days before the set-point change. Figures 7 present the initial conditions, the simulated and measured results at different positions (close to the OSB board, within the insulation layer or behind the rainscreen membrane). Temperatures and heat flux density are well predicted by the model, even when the transition is sharp during the first hours after the set-point change.

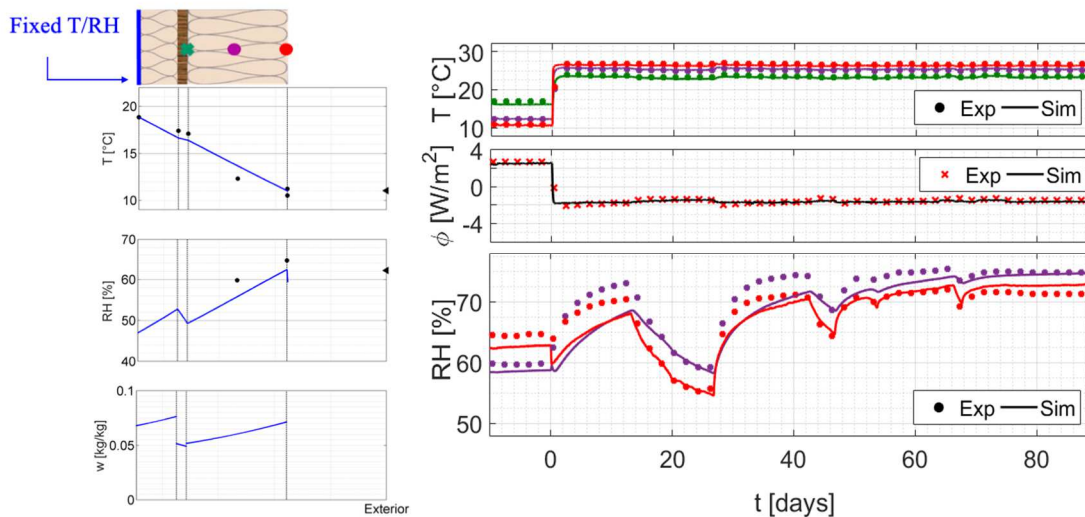


**Figure 7 : Initial conditions (a) and measured and simulated hygrothermal behavior (b) of Biobased system during hygrothermal safe test.**

Regarding relative humidity, differences do not exceed 2.5 % under steady-state, i.e. before the set-point change and after 60 days. During the transient stages, larger differences arise: the simulated sudden drop just after the set-point change is larger of 5 % than the measured one; simulated kinetics are slower during sorption stages, while a better agreement is observed during desorption stages.

In the view of improving the prediction, sensitivity analysis is carried out. Since wood wool sorption isotherms show hysteresis [44], the influence of its sorption capacity  $\theta$  is analyzed. Here,  $\theta$  is lowered since numerical studies including hysteresis of hygroscopic building materials showed that effective sorption capacity is lower than the ones of adsorption or desorption isotherms [34,36]. Results are presented in Figure 8. We observe that the RH increase is faster during the transient stages, improving the agreement with experimental results. The sensitivity of OSB sorption capacity and vapor diffusion resistance factors was also analyzed in [38], but their influence is much less significant.

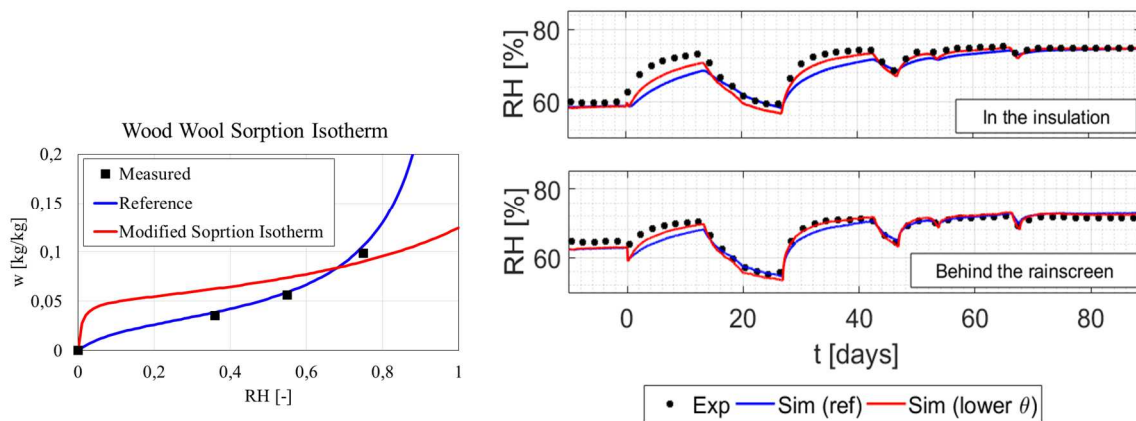


**Figure 8: Sorption isotherms for wood wool (a) and influence of wood wool sorption capacity on simulated relative humidity for Biobased system during hygrothermal safe test (b).**

Finally, the hygrothermal behavior of the entire wall (*RHCB wall* and *Biobased system*) is simulated. As good agreement is still observed for temperature and heat flow density [38],

only relative humidity variations are presented in Figure 9. An offset of 5 % and slightly different kinetics are observed at interface between *RHCB wall* and *Biobased* system. However, these differences have no influence on the hygrothermal behavior within *Biobased* system. Indeed, about 2/3 of hygric resistance of the entire wall is due to *RHCB wall*. Thus, *Biobased* system is less sensitive to interior than exterior conditions.

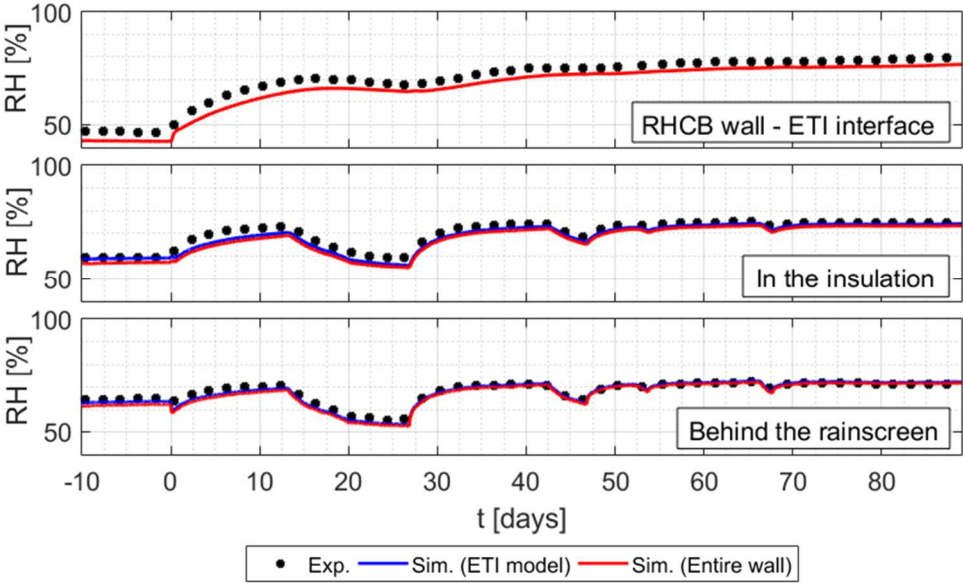


**Figure 9: Comparison of simulation approach on simulated relative humidity for *Biobased* system during hygrothermal safe test.**

Last, a similar methodology was applied for *Glass Wool*: satisfying results are still found for the prediction of temperature fields and heat flux density. As observed in Figure 10, a good agreement is also found for the relative humidity: here, the simulation results were less sensitive to insulation sorption capacity because of its less hygroscopic behavior, but more sensitive to OSB vapor diffusion resistance factor. Contrary to *Biobased* system, only small differences are observed at interface between *RHCB wall* and *Glass Wool* system.

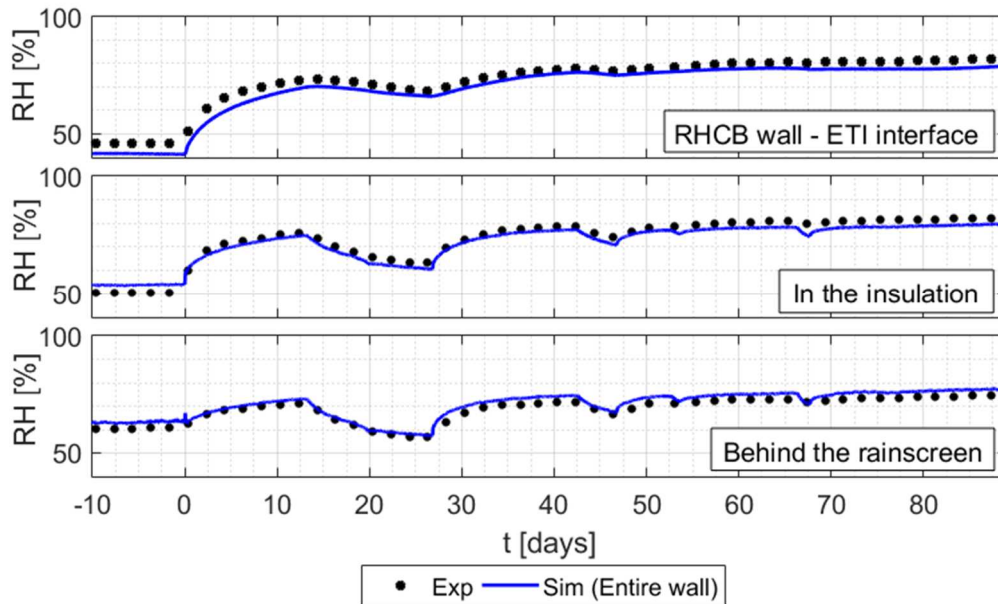


**Figure 10: Measured and simulated relative humidity for Glass Wool system during hygrothermal safe test.**

## 4.2 Interstitial condensation test

### 4.2.1 Comparison between numerical and experimental results

In the view of evaluating the model capacity on a wider domain, a scenario is defined by mean of steady-state analysis to lead theoretically to interstitial condensation around the interface between *RHCBC wall* and ETI systems. Exterior air temperature and relative humidity change respectively from 6 to 31 °C and from 70 to 80 % while interior air conditions are maintained at levels close to 19 °C and 70 %. The experiment was run for 35 days. The measured ambient conditions are reported on the Figure 11. Except a small decrease of exterior relative humidity around the 4<sup>th</sup> day, set-points are well respected.

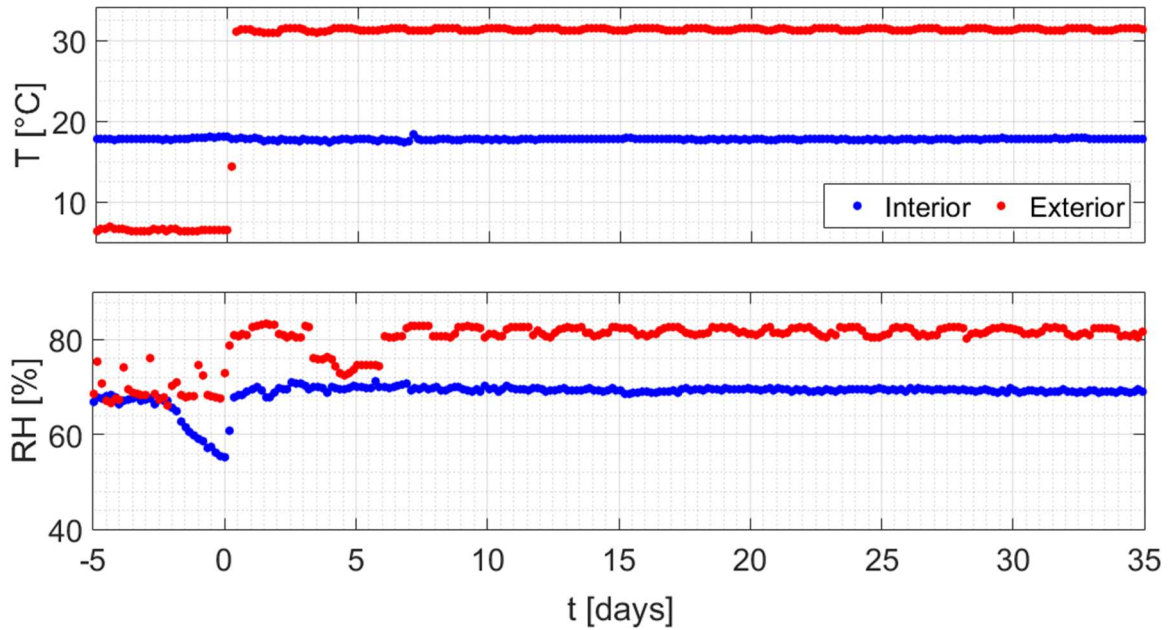


**Figure 11: Measured temperature and relative humidity at interior and exterior sides during interstitial condensation test.**

Measured and simulated relative humidity at different positions within the walls are presented in Figure 12. For *Glass Wool* system, measured relative humidity within or nearby insulation increases rapidly just after the solicitation and tends towards saturation levels. However, several failures occurred for the sensor placed at the wall-ETI interface, which led to a lack of data between the 1<sup>st</sup> and 31<sup>st</sup> days. After 35 days, saturation levels are reached, indicating effectively the presence of interstitial condensation. Consequently, relative humidity increases also in exterior cavities of the *RHCB wall*. Simulations catch the experimental behavior, except within the insulation. Glass wool is a low hygroscopic material (see Annex 1) for which determination of sorption isotherm at high relative humidity is rather difficult. Similar experimental and numerical observations are made for *Biobased* system. Last, by comparing both systems, measured and simulated relative humidity variations of *Biobased* system are more delayed and dampened. This is due to the higher hydric inertia and vapor diffusion resistance factor of the wood wool and the cellulose than the ones of glass wool.

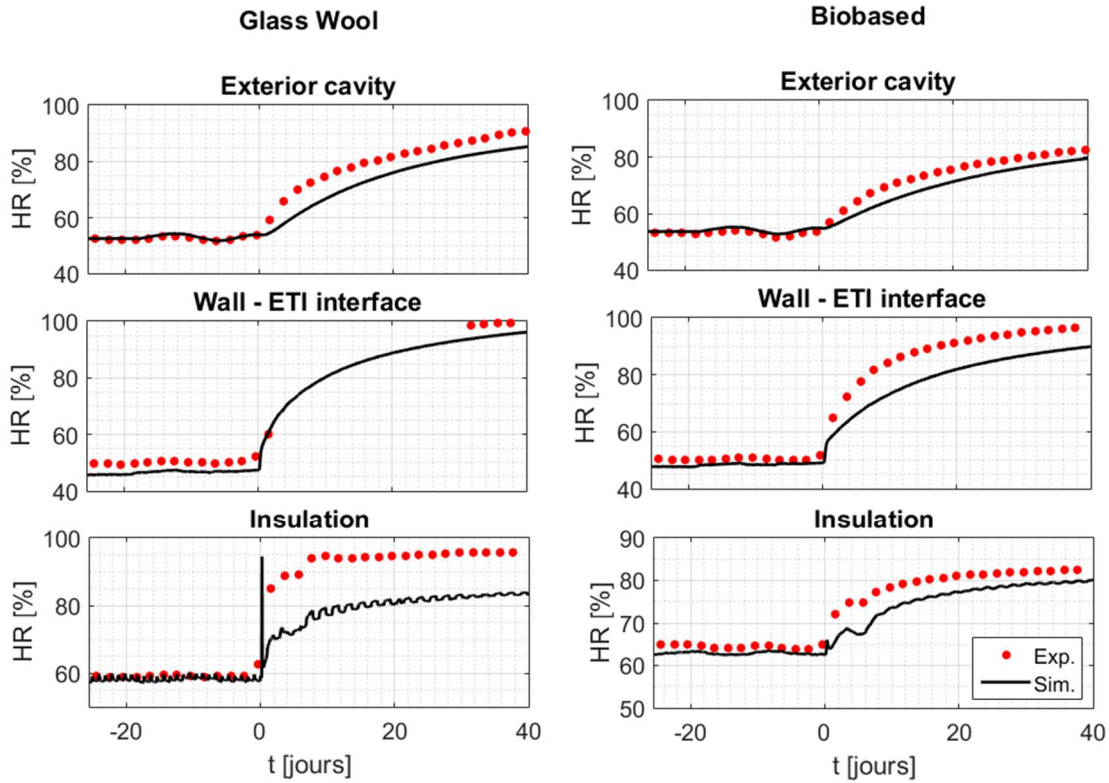


*Figure 12 : Measured and simulated relative humidity for the Biobased and Glass Wool system during interstitial condensation test.*

#### 4.2.2 Comparison of different ventilated cladding systems design

As mentioned in the introduction, few recommendations refer to hygrothermal behavior of ventilated cladding systems. Consequently, numerous ventilated cladding systems design may be found in the literature. However, the influence of design on wall durability is scarcely investigated in the literature. Since the model is validated on wide domain of temperature and relative humidity, four designs of ventilated cladding systems are studied in the view of evaluating the influence of rainscreen membrane and OSB board on interstitial condensation risk:

- Wall 0: with rainscreen membrane, with OSB board;
- Wall 1: without rainscreen membrane, with OSB board;
- Wall 2: with rainscreen membrane, without OSB board;

- Wall 3: without rainscreen membrane, without OSB board;
- Wall 4: with rainscreen membrane, with OSB board shifted 2 cm toward interior side.

Hygrothermal simulations are performed for *Biobased* and *Glass Wool* systems exposed to the previous scenario (see Figure 11). Table 3 focus particularly on the time to reach two critical relative humidity levels (80 % and 99 %) at the interface between *RHCB wall* and ETI systems. Whatever the wall configuration, critical relative humidities are reached more quickly for *Glass Wool* system than for *Biobased* system, as observed and explained before. Nevertheless, both systems present similar trends. For a target relative humidity of 80 %, OSB board has more influence than rainscreen membrane: removing OSB board reduces the critical time by 30-35 % instead of 12-14 % when removing rainscreen membrane; furthermore, shifting OSB board towards interior side allow delaying the critical time. On the other hand, OSB board and rainscreen membrane have similar influence when target relative humidity is 99 %: removing both elements may reduce the critical time by more than 70 %.

	RH	Wall 0	Wall 1	Wall 2	Wall 3	Wall 4
<i>Biobased</i>	80 %	16.7	14.7 (-12 %)	11.7 (-30 %)	9.5 (-43 %)	18.3 (+ 10 %)
	99 %	174	81.4 (-53 %)	78.8 (-55 %)	40.4 (-77 %)	170 (-2 %)
<i>Glass Wool</i>	80 %	10.5	9 (-14 %)	6.8 (-35 %)	5.8 (-45 %)	12 (+ 14 %)
	99 %	58.8	31.5 (-46 %)	31.7 (-46 %)	16.8 (-71 %)	57 (-3 %)

*Table 3: Time (in day) to reach critical relative humidity levels for different ventilated cladding systems design and deviation from the reference wall.*

## 5 Conclusions

This work focused on the hygrothermal behavior of three external thermal insulation systems. Experimentally, a rendered hollow concrete wall was insulated with one ETICS and two ventilated cladding systems among which one includes biobased insulation. The walls were tested in a bi climatic chamber in which temperature and relative-humidity are controlled. Simultaneously, their hygrothermal behavior were simulated with a heat and moisture transfer model under steady and transient states.

Regarding the thermal behavior, numerical results matched well with experimental data, whether for thermal resistance and temperature profiles or for transient temperature variations. Furthermore, all systems allow reducing heat fluxes and are therefore good candidate for improving building energy performance.

On the other hand, the hygric behavior depends on the system. For ETICS, experimental results highlighted that the adhesive used for installing the system provide a significant moisture source during the application and forms an additional moisture transfer resistance within the wall. In the present experimental set-up, hygrothermal equilibrium could not be reached for ETICS even after 160 days under favorable drying conditions. Under less favorable drying conditions (*i.e.* under real climate), it can be expected that moisture level remain high at the interface between initial wall and ETICS and, thus, that the durability of the renovated envelope is probably lowered. This should be particularly true if the initial wall is wet. Nevertheless, this point should be confirmed by a further numerical and experimental study.

Concerning ventilated cladding systems, a good agreement is found under steady-state. The transient behavior was evaluated for two cases: one leading to hygrothermal safe conditions

within the walls and one leading to interstitial condensation. For both cases, numerical results match with experimental data, but they are sensitive to insulation sorption capacity and OSB vapor diffusion resistance factor. Last, it was shown by numerical simulation that the design of ventilated cladding systems is of high importance regarding the risk of interstitial condensation: because of their higher sorption capacity biobased insulation may delayed and reduce this risk. In addition, we observed that OSB board and rainscreen membrane are essential to keep safe conditions within the wall. Nevertheless, the observed moisture related risks occurred only after 5 days of extreme condition at least. Therefore, it could be interesting to extend this study on the design for a wall subjected to real climatic solicitations.

## 6 References

- [1] <http://webtool.building-typology.eu/>
- [2] Ibañez-Puy, M., Vidaurre-Arbizu, M., Sacristán-Fernández, J. A., & Martín-Gómez, C. (2017). Opaque Ventilated Façades: Thermal and energy performance review. *Renewable and Sustainable Energy Reviews*, 79, 180-191.
- [3] Marinosci, C., Semprini, G., & Morini, G. (2014). Experimental analysis of the summer thermal performances of a naturally ventilated rainscreen façade building. *Energy and Buildings*, 72, 280-287.
- [4] Stazi, F., Ulpiani, G., Pergolini, M., Magni, D., & Di Perna, C. (2018). Experimental Comparison Between Three Types of Opaque Ventilated Facades. *The Open Construction and Building Technology Journal*, 12(1).
- [5] Pereira, C., de Brito, J., & Silvestre, J. D. (2018). Contribution of humidity to the degradation of façade claddings in current buildings. *Engineering Failure Analysis*, 90, 103-115.
- [6] Kvande, T., Bakken, N., Bergheim, E., & Thue, J. (2018). Durability of ETICS with Rendering in Norway—Experimental and Field Investigations. *Buildings*, 8(7), 93.
- [7] Barreira, E., & de Freitas, V. P. (2013). Experimental study of the hygrothermal behaviour of External Thermal Insulation Composite Systems (ETICS). *Building and environment*, 63, 31-39.
- [8] Zillig, W., Lenz, K., Sedlbauer, K., & Krus, M. (2003, September). Condensation on facades—influence of construction type and orientation. In *Proceedings of the 2nd International Conference on Building Physics, Leuven, Belgium* (pp. 437-444).

- [9] Barreira, E., Delgado, J. M. P. Q., Ramos, N. M. M., & de Freitas, V. P. (2013). Exterior condensations on facades: numerical simulation of the undercooling phenomenon. *Journal of Building Performance Simulation*, 6(5), 337-345.
- [10] Barreira, E., & de Freitas, V. P. (2014). The effect of nearby obstacles in surface condensations on external thermal insulation composite systems: experimental and numerical study. *Journal of Building Physics*, 37(3), 269-295.
- [11] Kočí, V., Maděra, J., & Černý, R. (2012). Exterior thermal insulation systems for AAC building envelopes: Computational analysis aimed at increasing service life. *Energy and Buildings*, 47, 84-90.
- [12] Kunzel, H. M. (1998). Effect of interior and exterior insulation on the hygrothermal behaviour of exposed walls, *Materials and Structures*, 31, 99–103.
- [13] Hradil, P., Toratti, T., Vesikari, E., Ferreira, M., & Häkkinen, T. (2014). Durability considerations of refurbished external walls. *Construction and Building Materials*, 53, 162-172.
- [14] Ilomets, S., Kalamees, T., Lahdensivu, J., & Klõšeiko, P. (2016). Impact of ETICS on corrosion propagation of concrete facade. *Energy Procedia*, 96, 67-76.
- [15] Orosz, M. (2012). Comparison of ETICS and ventilated cladding system in terms of hygrothermal loads of mineral wool in Middle-Europe. In *Proceedings of the Conference of Junior Researchers in Civil Engineering* (pp. 158-162).
- [16] Soares, N., Martins, C., Goncalves, M., Santos, P., da Silva, L. S., & Costa, J. J. (2018). Laboratory and in-situ non-destructive methods to evaluate the thermal transmittance and behaviour of walls, windows, and construction elements with innovative materials: a review. *Energy and Buildings*.

- [17] Rodrigues, L., White, J., Gillott, M., Braham, E., & Ishaque, A. (2017). Theoretical and Experimental Thermal Performance Assessment of an Innovative External Wall Insulation System for Social Housing Retrofit. *Energy and Buildings*, 162, 77-90.
- [18] Daniotti, B., Paolini, R., & Cecconi, F. R. (2013). Effects of ageing and moisture on thermal performance of ETICS cladding. In *Durability of Building Materials and Components* (pp. 127-171). Springer, Berlin, Heidelberg.
- [19] Xiong, H., Xu, J., Liu, Y., & Wang, S. (2016). Experimental study on hygrothermal deformation of external thermal insulation cladding systems with glazed hollow bead. *Advances in Materials Science and Engineering*, 2016, 1-13.
- [20] Xiong, H., Xu, J., & Yuan, K. (2018). Experimental study on the temperature field of ETICS cladding system with finishing colorful steel plate. *Journal of Building Engineering*, 18, 438-447.
- [21] Sala, J. M., Urresti, A., Martín, K., Flores, I., & Apaolaza, A. (2008). Static and dynamic thermal characterisation of a hollow brick wall: Tests and numerical analysis. *Energy and Buildings*, 40(8), 1513-1520.
- [22] Palumbo, M., Lacasta, A. M., Giraldo, M. P., Haurie, L., & Correal, E. (2018). Bio-based insulation materials and their hygrothermal performance in a building envelope system (ETICS). *Energy and Buildings*, 174, 147-155.
- [23] Palomar, I., Barluenga, G., Ball, R. J., & Lawrence, M. (2019). Laboratory characterization of brick walls rendered with a pervious lime-cement mortar. *Journal of Building Engineering*, 23, 241-249.
- [24] Hens, H., & Carmeliet, J. (2002). Performance prediction for masonry walls with EIFS using calculation procedures and laboratory testing. *Journal of Thermal Envelope and Building Science*, 25(3), 167-187.

- [25] Barreira, E., Delgado, J. M., Ramos, N. M. M., & De Freitas, V. P. (2012). Drying Kinetics of External Thermal Insulation Composite Systems (ETICS). *Defect and Diffusion Forum*, 326, 662-667.
- [26] Busser, T., Berger, J., Piot, A., Pailha, M., & Woloszyn, M. (2018). Experimental validation of hygrothermal models for building materials and walls: an analysis of recent trends.
- [27] Capener, C. M., & Sandin, K. (2013). Performance of a Retrofitted 1950's Multi-Unit Residential Building—Measurements and Calculated Transient Hygrothermal Behaviour. In *Thermal Performance of the Exterior Envelopes of Whole Buildings XII International Conference*.
- [28] Colinart, T., Bendouma, M., & Glouannec, P. (2019). Building renovation with prefabricated ventilated façade element: A case study. *Energy and Buildings*, 186, 221-229.
- [29] Pihelo, P., & Kalamees, T. (2019). Commissioning of moisture safety of nZEB renovation with prefabricated timber frame insulation wall elements. *Wood Material Science & Engineering*, 1-8.
- [30] Marinosci, C., Strachan, P. A., Semprini, G., & Morini, G. L. (2011). Empirical validation and modelling of a naturally ventilated rainscreen façade building. *Energy and Buildings*, 43(4), 853-863.
- [31] Falk, J., & Sandin, K. (2013). Ventilated rainscreen cladding: Measurements of cavity air velocities, estimation of air change rates and evaluation of driving forces. *Building and Environment*, 59, 164-176.
- [32] Langmans, J., & Roels, S. (2015). Experimental analysis of cavity ventilation behind rainscreen cladding systems: A comparison of four measuring techniques. *Building and Environment*, 87, 177-192.

- [33] Tariku, F., Simpson, Y., & Iffa, E. (2015). Experimental investigation of the wetting and drying potentials of wood frame walls subjected to vapor diffusion and wind-driven rain loads. *Building and Environment*, 92, 368-379.
- [34] Lelievre, D., Colinart, T., & Glouannec, P. (2014). Hygrothermal behaviour of bio-based building materials including hysteresis effects: Experimental and numerical analyses. *Energy and Buildings*, 84, 617-627.
- [35] Krischer, O. (1963). *Die Wissenschaftlichen Grundlagen der Trocknungstechnik*, 2 Aufl. Springer, Berlin.
- [36] Colinart, T., Lelièvre, D., & Glouannec, P. (2016). Experimental and numerical analysis of the transient hygrothermal behavior of multilayered hemp concrete wall. *Energy and Buildings*, 112, 1-11.
- [37] Colinart, T., Glouannec, P., Bendouma, M., & Chauvelon, P. (2017). Temperature dependence of sorption isotherm of hygroscopic building materials. Part 2: Influence on hygrothermal behavior of hemp concrete. *Energy and Buildings*, 152, 42-51.
- [38] Bendouma, M. (2018). *Systèmes d'Isolation par l'Extérieur : études expérimentales et numériques des transferts de chaleur et d'humidité* (PhD. Thesis, Université Bretagne Sud).
- [39] ISO 9869-1 (2014). *Thermal insulation – Building elements – In-situ measurement of thermal resistance and thermal transmittance, Part 1: Heat flow meter method*.
- [40] ISO 6946 (2007). *Building components and building elements—Thermal resistance and thermal transmittance—Calculation method*.
- [41] Laaroussi, N., Lauriat, G., Raefat, S., Garoum, M., & Ahachad, M. (2017). An example of comparison between ISO Norm calculations and full CFD simulations of thermal performances of hollow bricks. *Journal of Building Engineering*, 11, 69-81.
- [42] Hens, H. S. (2016). *Applied building physics: ambient conditions, building performance and material properties*. John Wiley & Sons.

- [43] Ozisik, M. N. (1985). Heat transfer: a basic approach.
- [44] Vololonirina, O., Coutand, M., & Perrin, B. (2014). Characterization of hygrothermal properties of wood-based products—Impact of moisture content and temperature. *Construction and Building Materials*, 63, 223-233.
- [45] ISO 12667 (2001). Thermal performance of building materials and products. Determination of thermal resistance by means of guarded hot plate and heat flow meter methods. Products of high and medium thermal resistance.
- [46] ISO 12572 (2016). Hygrothermal performance of building materials and products—Determination of water vapour transmission properties.
- [47] ISO 12571 (2013). Hygrothermal performance of building materials and products – Determination of hygroscopic sorption properties.
- [48] Zaknoune, A., Glouannec, P., & Salagnac, P. (2012). Estimation of moisture transport coefficients in porous materials using experimental drying kinetics. *Heat and Mass Transfer*, 48(2), 205-215.
- [49] Zaknoune, A., Glouannec, P., & Salagnac, P. (2013). Identification of the liquid and vapour transport parameters of an ecological building material in its early stages. *Transport in porous media*, 98(3), 589-613.

## 7 Nomenclature

### Roman

$cp$	Specific Heat [ $\text{J.kg}^{-1}.\text{K}^{-1}$ ]
$C$	Volumetric heat capacity [ $\text{J.m}^{-3}.\text{K}^{-1}$ ]
$D_v^\phi$	Water vapor diffusion coefficient [ $\text{kg.m}^{-2}.\text{s}^{-1}$ ]
$D_v^T$	Water vapor thermodiffusion coefficient [ $\text{kg.m}^{-2}.\text{s}^{-1}.\text{K}^{-1}$ ]
$D_l^\phi$	Liquid water migration coefficient [ $\text{kg.m}^{-2}.\text{s}^{-1}$ ]
$D_{v0}$	Binary diffusion coefficient of water in air [ $\text{kg.m}^{-2}.\text{s}^{-1}$ ]
$h_{cv}$	Convection heat transfer coefficient [ $\text{W.m}^{-2}.\text{K}^{-1}$ ]
$k_m$	Convective mass transfer coefficient [ $\text{m.s}^{-1}$ ]
$L_{v0}$	Latent heat of vaporization at 0 °C [ $\text{J.kg}^{-1}$ ]
$M_v$	Molar mass of water [ $\text{kg.mol}^{-1}$ ]
$p_{v_{sat}}$	Saturation vapor pressure [Pa]
$R$	Universal gas constant [ $\text{J.mol}^{-1}.\text{K}^{-1}$ ]
$S$	Surface [ $\text{m}^2$ ]
$T$	Temperature [K]
$t$	Time [s]
$V$	Volume [ $\text{m}^3$ ]
$w$	Moisture content [ $\text{kg.kg}^{-1}$ ]
RHCB	Rendered Hollow Concrete Block
ETI	External Thermal Insulation
ETICS	External Thermal Insulation Composite System

### Greek

$\phi$	Relative humidity [%]
$\varphi_M$	Mass flux density [ $\text{kg.m}^{-2}.\text{s}^{-1}$ ]
$\varphi_T$	Heat flux density [ $\text{W.m}^{-2}$ ]
$\lambda$	Thermal conductivity [ $\text{W.m}^{-1}.\text{K}^{-1}$ ]
$\mu$	Vapor diffusion resistance factor [-]
$\theta$	Sorption capacity [-]
$\rho$	Density [ $\text{kg.m}^{-3}$ ]
$\varepsilon$	Emissivity [-]

$\sigma$  Stefan-Boltzmann constant [ $\text{J}\cdot\text{m}^{-2}\cdot\text{K}^{-4}$ ]

#### Subscripts

amb	Ambient
cav	Cavity
l	Liquid
rad	Radiative
ref	Reference
s	Solid
surf	Surface
v	Vapor

## 8 Annex 1

All materials have been characterized in the laboratory. Thermal properties are evaluated in dry state after drying at 60 °C. Thermal capacity  $c_p$  is determined by differential scanning calorimetric measurement ( $\mu$ -DSC III, Setaram, Caluire, France) in the range [5 – 35 °C]. Dry thermal conductivity  $\lambda_{dry}$  is measured at 23 °C by the guarded hot plate technique according to the standard ISO 12667 [45]. Long-wave emissivity is integrated in the range [2.5 – 25  $\mu$ m] with a spectrophotometer (FTIR-8000, Shimadzu, Kyoto, Japan) coupled with an integrating sphere. Dry cup experiments are conducted according to ISO 12572 [46] to assess vapor resistance factor  $\mu_{dry}$ . Last, sorption isotherms are determined gravimetrically at 23 °C in the hygroscopic domain (from 0 to 97 %) according to ISO 12571 [47] and fitted with GAB model:

$$w = \frac{w_m C K \phi}{(1 - K \phi)(1 - K \phi + C K \phi)} \quad (3)$$

with  $w_m$ ,  $C$  and  $K$  fitting parameters.

For all measurements, the uncertainty is in the order of 5 %. Results are gathered in Table 4, Table 5 and Figure 13.

Material	$\rho$ [kg.m <sup>-3</sup> ]	$c_p$ [J.kg <sup>-1</sup> .K <sup>-1</sup> ]	$\lambda_{dry}$ [W.m <sup>-1</sup> .K <sup>-1</sup> ]	$\mu_{dry}$ [-]	$\epsilon$ [-]
Concrete	1890	790	1.4	21.5	0.74
Plaster	1250-1600	810-840	0.32-0.44	31-10.6	0.75
Glass wool (Type 1)	15	870	0.042	2.4	
Glass wool (Type 2)	34	860	0.035	2.9	
Wood wool	47	1330	0.041	3.6	
Cellulose wadding	55	1200	0.044	-	
EPS	16	1210	0.036	37.4	
OSB board	560	1320	0.097	62	
Rainscreen membrane	-	-	-	433	0.7

*Table 4: Measured hygrothermal properties.*

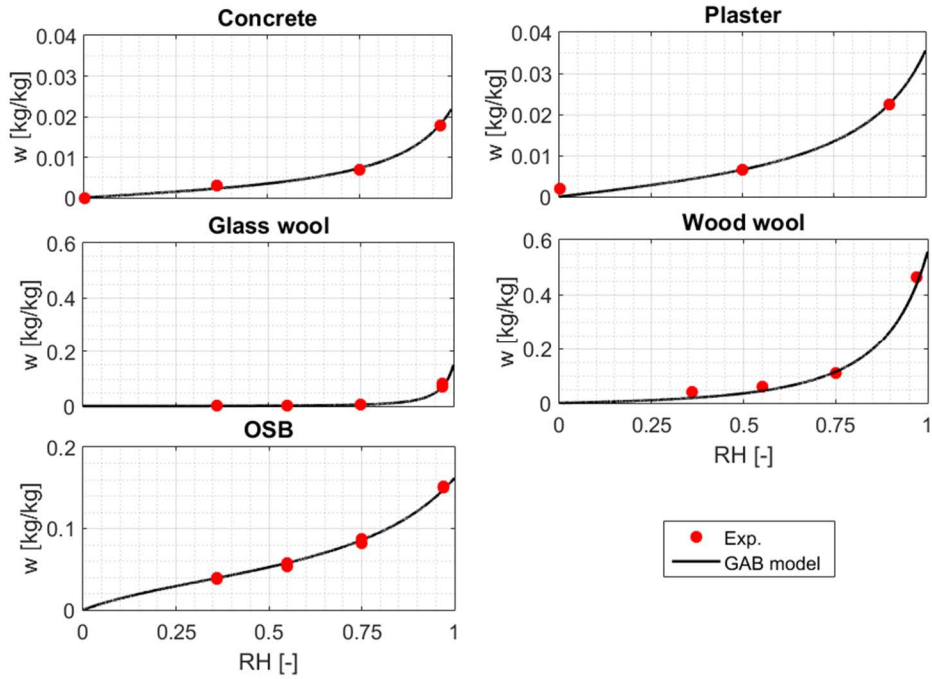


*Figure 13: Sorption isotherms.*

Material	$w_m$	$C$	$K$
Concrete	0.002	10	0.9
Plaster	0.003	10	0.9
Glass wool	0.002	10	0.99
Wood wool	0.03	10	0.97
OSB board	0.03	200	0.8

*Table 5: GAB fitting parameters.*

## 9 Annex 2

### 9.1 Heat and moisture transfer model in porous materials

A model of heat and moisture transfer within multilayered building materials was developed and validated in previous studies [34,36,37]. Here, hysteresis and temperature dependence of sorption isotherms and liquid thermomigration are neglected. Considering the temperature and the relative humidity as driving potentials, it comes:

$$\begin{aligned} & \rho_s (c p_s + w c p_l) \frac{\partial T}{\partial t} \\ & = -\nabla (-\lambda \nabla T) + \nabla \left( (D_v^\phi \nabla \phi + D_v^T \nabla T) (L_{v0} + (c p_v - c p_l)(T - T_{ref})) \right) \end{aligned} \quad (4)$$

$$\rho_s \theta \frac{\partial \phi}{\partial t} = -\nabla \left( -(D_l^\phi + D_v^\phi) \nabla \phi - D_v^T \nabla T \right) \quad (5)$$

Vapor diffusion coefficients  $D_v^\phi$ ,  $D_v^T$  and liquid migration coefficient  $D_l^\phi$  are expressed as:

$$D_v^\phi = \frac{D_{v0}}{\mu} \frac{M_v}{R T} p_{v_{sat}}(T) \quad (6)$$

$$D_v^T = \frac{D_{v0}}{\mu} \frac{M_v}{R T} \phi \left( \frac{d p_{v_{sat}}(T)}{dT} - \frac{p_{v_{sat}}(T)}{T} \right) \quad (7)$$

$$D_l^\phi = \theta \exp\left(p_1 + \frac{p_2}{w}\right) \quad (8)$$

With  $p_1$  and  $p_2$  two empirical coefficients [48,49].

This model applies to the solid part of hollow concrete block and all other solid materials. At the interface between two materials, a perfect contact is assumed which lead to the continuity of temperature and vapor pressure fields.

### 9.2 Energy and mass balances in hollow concrete block cavities

By assuming homogeneous air in the hollow concrete block cavities, energy and mass balances write:

$$\left( V_{cav} C_{cav} \frac{dT_{cav}}{dt} + (L_{v0} + c_{pv} (T_{cav} - T_{ref})) \frac{dm_{v,cav}}{dt} \right) = \sum (\varphi_{T,cav} S_{cav}) \quad (9)$$

$$\frac{dm_{v,cav}}{dt} = \sum (\varphi_{m,cav} S_{cav}) \quad (10)$$

Where  $\varphi_{T,cav}$  and  $\varphi_{m,cav}$  are respectively heat and mass flux densities exchanged between air cavity and the surrounding surfaces (see Figure 2):

$$\varphi_{T,cav} = h_{cv} (T_{surf,cav} - T_{cav}) + \varphi_{m,cav} L_v \quad (11)$$

$$\varphi_{m,cav} = k_m \left( \frac{M_v}{R} \right) \left( \frac{\phi_{surf,cav} p_{v,sat}(T_{surf,cav})}{T_{surf,cav}} - \frac{\phi_{cav} p_{v,sat}(T_{cav})}{T_{cav}} \right) \quad (12)$$

Note that long-wave radiation exchange occurs between surfaces of hollow concrete block cavities. Therefore, heat fluxes for these surfaces write:

$$\varphi_{T_{surf,cav}} = h_{rad} (T_{surf,1} - T_{surf,2}) + \varphi_{T,cav} \quad (13)$$